Environmental Science and Pollution Research (2023) 30:71957–71969
https://doi.org/10.1007/s11356-022-22746-x

Synthesis and characterization of NiO/Cr_2O_3 nanocomposite with effective sunlight driven photocatalytic degradation of organic dyes

Sapna Yadav[1] · Nutan Rani[1] · Kalawati Saini[1]

Received: 19 May 2022 / Accepted: 22 August 2022 / Published online: 30 August 2022

Abstract

In this paper, nanocomposite NiO/Cr_2O_3 has been synthesized by a simple chemical reduction method to study its photocatalytic activity under sunlight irradiation. Various advanced analytical techniques including powder X-ray diffraction (PXRD), scanning electron microscopy (SEM), transmission electron microscopy (TEM), energy-dispersive spectroscopy (EDS), elemental mapping, Fourier transform infrared spectroscopy (FTIR), and UV-visible spectroscopy have been utilized to characterize the synthesized NiO/Cr_2O_3 nanocomposite. SEM images show the sheet-shaped morphology of NiO/Cr_2O_3 nanocomposite. These sheets have a rough surface with nano to micro size cracks. These cracks play important role in the enhancement of photocatalytic activity by increasing surface active sites for the adsorption of dye molecules on the surface of the photocatalyst. The organic dyes crystal violet (CV) and methylene blue (MB) have been chosen to study the photocatalytic behavior of NiO/Cr_2O_3 nanocomposite under sunlight irradiation. The photocatalytic efficiency of NiO/Cr_2O_3 nanocomposite has been obtained 88.47% and 93.63% against crystal violet and methylene blue respectively. The results of the photocatalytic kinetics exhibit that degradation rate constant value for crystal violet dye is higher as compared to methylene blue dye. Obtained kinetic results indicate that synthesized nanocomposite acts as an efficient photocatalyst for the degradation of both crystal violet dye and methylene blue dye. NiO/Cr_2O_3 nanocomposite also exhibited reusability and stability for photocatalytic degradation of both organic dyes. Photoelectrochemical measurements as photocurrent, electrochemical impedance spectroscopy (EIS), and Mott-Schottky plot were also performed for synthesized NiO/Cr_2O_3 nanocomposite. Consequently, this synthesized NiO/Cr_2O_3 nanocomposite can be utilized for environmental remediation of harmful dyes.

Keywords Nanocomposite · NiO/Cr_2O_3 · Nanosize cracks · Microsize cracks · Photocatalytic · Degradation

Introduction

In the current era, environmental pollution caused by the discharge of textile industries sewage including toxic organic dyes is a matter of serious concern. Therefore, the elimination of organic dyes before the discharge of industrial wastewater is still a challenge for researchers (He et al. 2010). Various technologies have been utilized for wastewater treatment nowadays such as aerobic biodegradation, chlorination, liquid-liquid extraction, activated carbon adsorption, membrane filtration and adsorption, and photocatalytic degradation. Among them, photocatalytic degradation of toxic organic dyes into harmless compounds under light is a simple, green, cost-efficient, and promising process (Ranjith et al. 2019; Dewangan et al. 2020). Semiconductor-based nanoparticles have attracted considerable attention with their potential applications in various fields. The hydrothermal method has been reported for the synthesis of transition metal oxide semiconductor CdO-ZnO nanocomposite. That synthesized nanocomposite showed efficient removal of rhodamine B dye (Mahendiran et al. 2019). Hong et al. have used graphene oxide (GO)/V_2O_3 and GO/TiO_2 composites for hydrogen storage (Hong et al. 2012). Liu et al. have synthesized NiO/MnO_2 nanocomposite for flexible supercapacitor application (Liu et al. 2018). Rahman et al. have reported selective chloroform sensing property of NiO/multi-walled carbon nanotubes (MWCNT) nanocomposite (Rahman et al.

Responsible Editor: Sami Rtimi

✉ Kalawati Saini
kalawati.saini@mirandahouse.ac.in

[1] Department of Chemistry, Miranda House, University of Delhi, Patel Chest Marg, New Delhi 110007, India

2016). Photocatalytic evolution of H_2 has been studied by Pt-loaded Zinc vacancies in ZnO–ZnS system (Liu et al. 2021b). Herein, the production of an intermediate energy level takes place because of the presence of zinc vacancies, the introduction of Pt single atoms promotes the type-V electron transport from the conduction band (CB) of ZnO to the intermediate energy level and after that to the Pt atom. The type-V electron transport not only plays a key role in having a high reduction potential of photogenerated electrons but also prohibits the recombination of carriers. The synthesis of the Ni/C/Al_2O_3 framework and its successful use as a catalyst has been reported for the reduction of perfluoroalkyl carboxylic acid from wastewater (Liu et al. 2021a). The production of H_2 via selective oxidation of benzyl alcohol to benzaldehyde has been reported using VC/CdS (vanadium carbide/cadmium sulfide) nanowires (Tayyab et al. 2022). Semiconductors are the most preferred photocatalysts for the degradation of organic dyes due to their chemical properties, physical properties, and energy bandgap (Zhang et al. 2019). There is a formation of electron and hole pair by light radiation on the surface of semiconductor photocatalyst due to its suitable energy bandgap. This electron and hole pair further bring out a radical chain reaction for the photocatalytic degradation of toxic organic dyes into non-toxic compounds (Zhu and Zhou 2019; Abukhadra et al. 2018).

Transition metal oxide semiconductor-based nanocomposites are widely investigated for enhanced photocatalytic degradations of organic dyes. These nanocomposites have been synthesized using different synthesis methods. For example, Co_3O_4/ZnO nanocomposite-based photocatalyst has been synthesized using a microwave-assisted method (Hassanpour et al. 2017). ZnO/graphene nanocomposite has been synthesized using a one-step kinetic spray process. Synthesized ZnO/graphene nanocomposite has efficiently degraded methylene blue dye solution (Abd-Elrahim and Chun 2021). ZnO/TiO_2 photocatalyst has been fabricated by anodizing and calcinations (Hou et al. 2021). ZnO/TiO_2 nanocomposite has also been synthesized using the sol-gel method. ZnO/TiO_2 nanocomposite has shown photocatalytic degradation of methylene blue dye (Din et al. 2018).

NiO and Cr_2O_3 transition metal oxides are p-type semiconductors with energy bandgaps of 3.6 to 4.0 eV for NiO and ~3.4 eV for Cr_2O_3 respectively (Madkour et al. 2016; Rahimi-Nasarabadi et al. 2016). This wide energy bandgap of NiO is making it suitable for photocatalytic degradation of dye molecules (Aminuzzaman et al. 2021). The photocatalytic activity also depends on surface area (morphologies), particle size, and crystalline behavior (Aminuzzaman et al. 2021). Both NiO and Cr_2O_3 have similar properties (according to energy bandgap). Therefore, nanocomposites of both NiO and Cr_2O_3 show greater associated functionality than individual NiO and Cr_2O_3 semiconductors (Al-Hada et al. 2020). Because of this reason, we have tried to synthesize p-p junction NiO/Cr_2O_3 nanocomposite for enhancing its photocatalytic behavior against organic dyes.

Different approaches for the preparation of NiO/Cr_2O_3 nanocomposite have been reported in the literature such as a facile hydrothermal method (Maheshwaran et al. 2021), combustion method (Krishna et al. 2018), and co-precipitation method (Zoromba et al. 2019; Ma et al. 2015), evaporation and drying method (Mohammad et al. 2020), etc. These methods of nanocomposite synthesis have some disadvantages such as synthesis at high-temperature, use of hazardous reagents, production of chemical wastes, and others.

In this study, a simple two-step chemical reduction method is used for the synthesis of NiO/Cr_2O_3 nanocomposite, where harmless tri-sodium citrate is used as stabilizing agent/capping agent and reaction is occurred under low-temperature conditions. The comparative photocatalytic activities of synthesized NiO/Cr_2O_3 nanocomposite are investigated against crystal violet (CV) and methylene blue (MB) dyes under sunlight irradiation. Photocatalytic stability of synthesized NiO/Cr_2O_3 nanocomposite has been checked for five cycles. We have also conducted photoelectrochemical measurements such as photocurrent, electrochemical impedance spectroscopy (EIS), and Mott-Schottky plot of synthesized NiO/Cr_2O_3 nanocomposite.

Experimental section

Materials

Nickel (II) acetate tetrahydrate ($Ni(CH_3COO)_2.4H_2O$, 98%, extra pure), Chromium (III) acetate anhydrous ($Cr(CH_3COO)_3$, 98%, extra pure), Sodium hydroxide (NaOH, 96%), Sodium sulfate anhydrous (Na_2SO_4, AR grade), Methylene blue (96%), and Crystal violet (96%) were purchased from Central Drug House (P) LTD. Trisodium citrate dihydrate (98%, extra pure) was purchased from Loba Chemie PVT. LTD. Carbon black (super P) and Pyrrolidinone (99 %) were purchased from Thermo Fisher Scientific Pvt. Lid. India. Poly(vinylidene fluoride) was purchased from Sigma Aldrich Chemie USA. All chemicals were used without any further purification and deionized water was used in all experiments.

Synthesis of NiO/Cr_2O_3 nanocomposite

NiO/Cr_2O_3 nanocomposite was synthesized through a simple two steps chemical reduction method. In the first step, 200 mM of trisodium citrate dihydrate was added to 50 mL of 0.2 M nickel (II) acetate tetrahydrate aqueous solution. Then, 50 mL of 2.0 M sodium hydroxide aqueous solution was added to the above solution with stirring. The obtained precursor solution was heated at 40 °C with stirring for one hour using

a hot plate magnetic stirrer. After that in the second step, a 50 mL solution of 0.2 M chromium (III) acetate anhydrous was added drop-wise into the reaction solution followed by heating for another two hours by maintaining the same reaction conditions. Finally, the obtained sample was washed with deionized water and ethyl alcohol and dried at 80 °C for 5 h. The obtained sample was then placed in a furnace for calcination at 700 °C for 8 h to get NiO/Cr_2O_3 nanocomposite.

Characterizations of NiO/Cr_2O_3 nanocomposite

Powder X-ray diffraction (PXRD) data were collected from the Bruker AXS D8 Discover instrument (Cu Kα radiation, λ = 1.54184 Å). Scanning electron microscopy (SEM), energy-dispersive spectroscopy (EDS), and elemental mapping analysis were performed by using a JEOL scanning electron microscope (SEM coupled with EDS, Japan model: JSM6610LV) at accelerating voltage and magnification of 20 kV and X 27,000 respectively. Transmission electron microscopy (TEM) analysis was performed by using a JEOL, Transmission electron microscope (JEM-F200) at 100 Kx magnification and 200 kV accelerating voltage, Fourier transform infrared spectroscopy (FTIR) was examined on the Perkin Elmer FTIR spectrometer with ATR & Specular reflectance for the determination of functional groups of the synthesized nanocomposite. Spectramax M2e UV-visible spectrophotometer was used to record the UV-Visible spectrum.

Photocatalytic activity of NiO/Cr_2O_3 nanocomposite

Photocatalytic activity of synthesized NiO/Cr_2O_3 nanocomposite was explored against the degradation of crystal violet (CV) and methylene blue (MB) dyes. The degradation experiments were carried out for both the abovementioned dyes separately in the absence and presence of NiO/Cr_2O_3 nanocomposite. Herein, 50 mL of 10 ppm aqueous dye solutions (both CV and MB separately) was irradiated under sunlight for 30 min in absence of NiO/Cr_2O_3 nanocomposite. After that, the photocatalytic degradation experiments were performed with 50 mg of NiO/Cr_2O_3 nanocomposite separately under sunlight within 30 min for CV and 180 min for MB respectively. The former mixtures of dye solutions and NiO/Cr_2O_3 nanocomposite were stirred in dark for 20 min to achieve adsorption-desorption equilibrium before being irradiated by natural sunlight. Dyes samples were collected at regular intervals of time and analyzed using the UV-visible spectrophotometer (Spectramax M2e UV-visible spectrophotometer). Five cycles of experiments have been run for each dye to understand reusability of synthesized NiO/Cr_2O_3 nanocomposite as a photocatalyst.

Photoelectrochemical characterizations of NiO/Cr_2O_3 nanocomposite

Photoelectrochemical characterizations were observed using a CHI 760E electrochemical workstation. NiO/Cr_2O_3 nanocomposite, carbon black, and poly (vinylidene fluoride) in 8:1:1 ratio were taken in a mortar pestle and crushed together for few minutes. After that, 2 drops of pyrrolidinone were added to the above mixture as solvent and mixed well to get a uniform paste. The above paste was then uniformly spread on sheet of stainless steel having area of 1.0 cm^2. This NiO/Cr_2O_3 nanocomposite modified stainless steel electrode was then dried in a hot air oven at 60 °C. NiO/Cr_2O_3 nanocomposite modified stainless steel electrode was used as working electrode, Pt wire electrode was used as counter electrode, and Ag/AgCl electrode was used as reference electrode. All the photoelectrochemical measurements were performed in 0.5 M Na_2SO_4 electrolyte. The one-solar (100 mW/cm^2) Xenon lamp was used as light source. The photocurrent experiment was performed for the run time of 240 s at 0.5 V. The electrochemical impedance spectroscopy (EIS) experiment was performed under light at a frequency range of 1–10^5 Hz with amplitude of 0.005 V. The Mott-Schottky experiment was performed under light at a frequency 1000 Hz with amplitude of 0.005 V.

Results and discussion

Powder X-ray diffraction and UV-visible spectrum analysis of NiO/Cr_2O_3 nanocomposite

Powder X-ray diffraction (PXRD) analysis has been used to detect the crystalline phase of NiO/Cr_2O_3 nanocomposite. Figure 1a shows the PXRD pattern of NiO/Cr_2O_3 nanocomposite. The 2θ peaks have been obtained at 37.96°, 43.57°, 62.42°, 76.46°, and 79.22° respectively. These 2θ values have been indexed corresponding to hkl planes (111), (200), (220), (311), and (222) respectively for synthesized NiO (Srirattanapibul et al. 2022). The 2θ peaks have been determined for synthesized Cr_2O_3 at 23.91°, 34.21°, 35.33°, 39.98°, 41.51°, 44.52°, 50.40°, 54.83°, 58.97°, 65.44°, 67.26°, 73.43°, 78.44°, and 80.57° respectively. Their corresponding hkl planes have been assigned as (012), (104), (110), (006), (113), (202), (024), (116), (122), (214), (300), (010), (220), and (306) respectively. These data are found to be similar to the reported values in the literature (Fu et al. 2015; Al-Hada et al. 2020). Obtained powder X-ray diffraction patterns of the sample confirm the presence of crystalline phase of nanocomposite NiO/Cr_2O_3 along with some impurity peaks. Obtained PXRD pattern has been matched with its cubic structure (JCPDS No. 47-1049) for NiO NPs

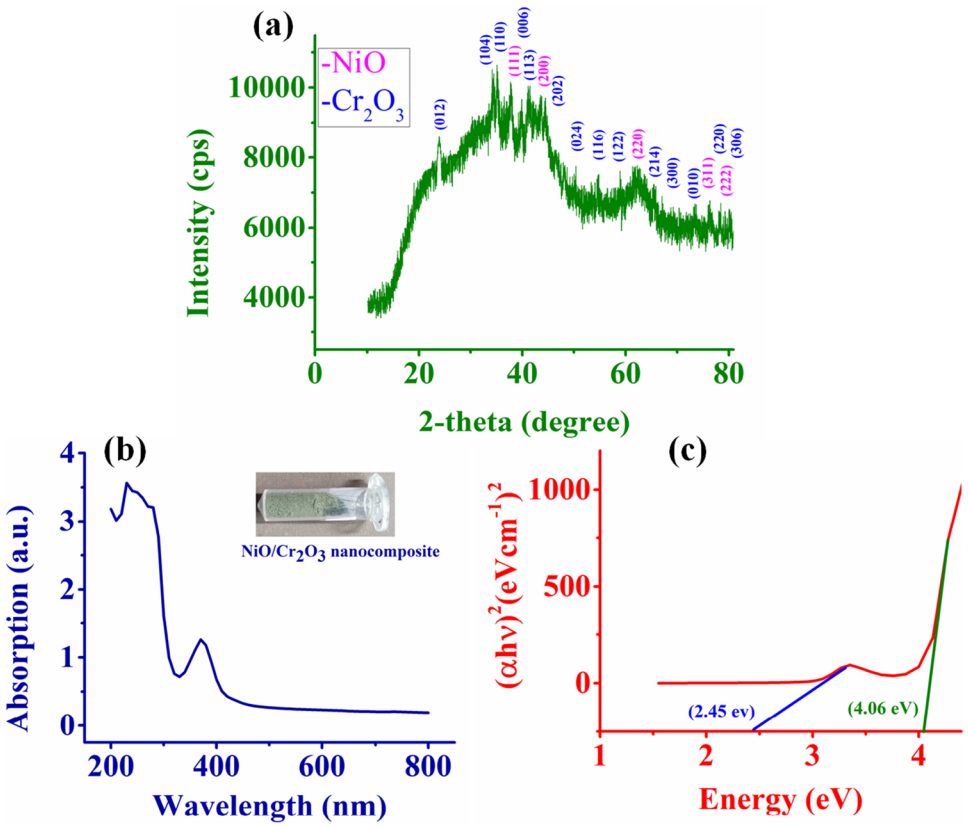

Fig. 1 (**a**) Powder X-ray diffraction (PXRD) of NiO/Cr_2O_3 nanocomposite, (**b**) UV-visible absorbance spectrum of NiO/Cr_2O_3 nanocomposite, and (**c**) Tauc's plots $(\alpha h\nu)^2$ vs hν of NiO/Cr_2O_3 nanocomposite

and with the hexagonal structure (JCPDS No. 38-1479) for Cr_2O_3 NPs.

Figure 1b shows the UV-visible spectrum recorded in the wavelength of range 200–800 nm. The absorption maxima have been obtained at 230 nm and 370 nm for Cr_2O_3 (Singh et al. 2017) and NiO (Alagiri et al. 2012) respectively. The values of the energy bandgap of the synthesized NiO/Cr_2O_3 nanocomposite have been determined using Tauc's equation, as given below.

$$(\alpha h\nu) = A\left(h\nu - E_g\right)^n \quad (1)$$

Where α is the absorption coefficient, hν is the photon energy, A is a constant, E_g is the bandgap energy of the material and n is an exponent ($n = 1/2$ for allowed direct transition and $n = 2$ for allowed indirect transition). Equation (1) is given in the literature (Barir et al. 2017). Tauc's plot is shown in Fig. 1c. Calculated bandgap energy values are 2.45 eV for Cr_2O_3 and 4.06 eV for NiO. Similar values of bandgap energy are also reported in the literature (Al-Hada et al. 2020; Al-Hada et al. 2021). Cr_2O_3 exhibits a decrease in energy bandgap value than bulk Cr_2O_3 due to defects. These defects are interstitials defect or vacancy defects (Guillén and Herrero 2021), whereas NiO exhibits a slight blue shift due to the decrease in particle size and quantum confinement (Alagiri et al. 2012).

Scanning electron microscopic, transmission electron microscopic, elemental mapping and energy-dispersive spectroscopic analysis of NiO/Cr_2O_3 nanocomposite

Scanning electron microscopic (SEM) and transmission electron microscopic (TEM) analysis reveal the surface morphology and size of synthesized NiO/Cr_2O_3 nanocomposite. Figure 2 represents the scanning electron micrographs and transmission electron micrographs of NiO/Cr_2O_3 nanocomposite. As it is evident from the SEM images, Fig. 2a and Fig. 2b are the zoom-out parts of an SEM image in Fig. 2c. The synthesized NiO/Cr_2O_3 nanocomposite has sheet-shaped morphology. These sheets are with rough surfaces and micro-sized to nano-sized cracks. There are also a few external growths on the surface of the sheets. The crack sizes of the NiO/Cr_2O_3 nanocomposite have been observed in the range of ~25 to ~500 nm (as marked in Fig. 2a and Fig. 2b). The possible reason for these cracks is heating at a high temperature (700 °C). The cracked morphology of synthesized NiO/Cr_2O_3 nanocomposite is also confirmed by the TEM image presented in Fig. 2d. The selected area electron diffraction (SAED) pattern of synthesized NiO/Cr_2O_3 nanocomposite with concentric circles reveals its crystalline nature (Rani et al. 2021). Due to the presence of cracks, the surface area of NiO/Cr_2O_3 nanocomposite has increased

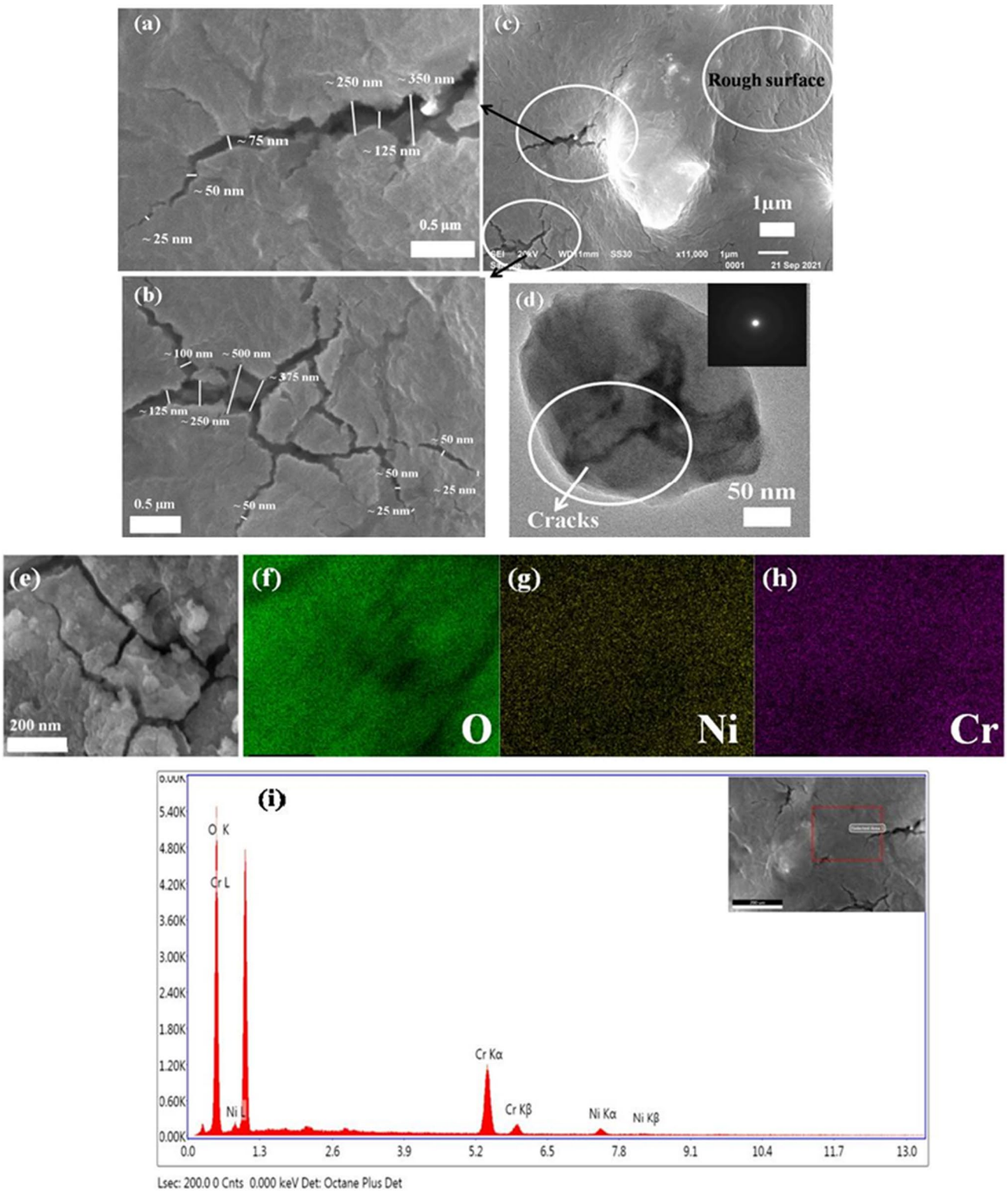

Fig. 2 (**a**), (**b**), (**c**) SEM images of synthesized NiO/Cr_2O_3 nanocomposite, (**d**) TEM image of synthesized NiO/Cr_2O_3 nanocomposite, (**e**) is selected area of synthesized NiO/Cr_2O_3 nanocomposite for elemental mapping, (**f**), (**g**), (**h**) elemental mapping images (O, Ni, and Cr respectively), and (**d**) energy-dispersive spectroscopy (EDS) of synthesized NiO/Cr_2O_3 nanocomposite

Table 1 Energy-dispersive spectroscopy (EDS) analysis

Element	Weight %	Atomic %	Net Int.	Error %
O K	55.08	80.21	160.46	4.26
Cr K	38.40	17.20	76.02	2.64
Ni K	6.52	2.59	6.93	13.68

which further enhanced the photocatalytic activity against MB and CV organic dyes. The heat treatment has also been used to induce nano-cracks in CeO_2-TiO_2 hybrid nanostructures (Veziroglu et al. 2019). EDS and elemental mapping analysis also confirm the synthesis of NiO/Cr_2O_3 nanocomposite. Figure 2f, g, h presents the elemental mapping of O, Ni, and Cr in synthesized NiO/Cr_2O_3 nanocomposite (selected area for elemental mapping is given in Fig. 2e). The elemental mapping of synthesized NiO/Cr_2O_3 nanocomposite confirms the uniform distribution of O, Ni, and Cr elements. The EDS analysis of synthesized NiO/Cr_2O_3 nanocomposite is reported in Fig. 2i. The obtained peaks corresponding to Ni, Cr, and O elements are presented in NiO/Cr_2O_3 nanocomposite. The percentage elemental composition of NiO/ Cr_2O_3 nanocomposite has been determined with EDS analysis. Obtained data are given in Table 1. A small amount of Ni than Cr confirms the presence of Cr_2O_3 on the surface of NiO. Similar EDS data have been reported by Li et al. for ZnO/SiO_2 nanocmposite. Herein, SiO_2 is found on the surface of ZnO (Li et al. 2009).

Fourier transform infrared spectroscopy analysis of NiO/Cr_2O_3 nanocomposite

Attenuated total reflection Fourier transform infrared spectroscopy (ATR-FTIR) has been used for studying the functional groups present on the surface of the synthesized NiO/Cr_2O_3 nanocomposite. The FTIR spectrum of NiO/Cr_2O_3 nanocomposite has been recorded in the spectral range of 400–4000 cm^{-1} (Fig. 3). Obtained peaks between 418 and 877 cm^{-1} are due to metal oxide bond vibrations. The peak located at 1074 cm^{-1} is due to the bending vibration of water absorbed on the surface of NiO/Cr_2O_3 nanocomposite. The peaks observed at 1336 cm^{-1}, 1421 cm^{-1}, and 1558 cm^{-1} correspond to C–O stretching vibrations, C–H stretching vibrations, and C=O stretching vibrations of the carboxyl or carbonyl group respectively. The obtained peak at 1648 cm^{-1} and the broad absorption peak around 3295 cm^{-1} are due to OH stretching (Hema et al. 2013; Liang et al. 2012).

Evaluation of photocatalytic activity of NiO/Cr_2O_3 nanocomposite

Sunlight is a very abundant, eco-friendly, freely available and natural source of light (Pirzada et al. 2019). Therefore,

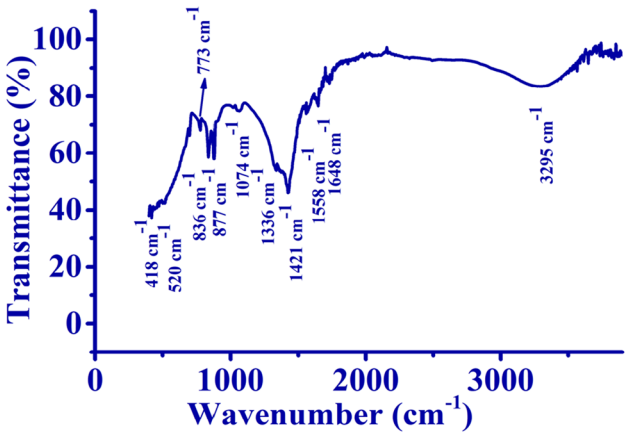

Fig. 3 FTIR spectrum of synthesized NiO/Cr_2O_3 nanocomposite

we have used natural sunlight as a light source for studying the photocatalytic activity with synthesized NiO/Cr_2O_3 nanocomposite. Fifty milliliters of (10 ppm) CV and 50 mL of (10 ppm) MB aqueous dye solutions have been used separately to monitor the photocatalytic activity of synthesized NiO/Cr_2O_3 nanocomposite under sunlight exposure. Two sets of experiments have been performed with each dye. The first experiment was performed in absence of NiO/Cr_2O_3 nanocomposite and the second experiment was performed in presence of NiO/Cr_2O_3 nanocomposite with both CV and MB dyes. Samples of dyes have been collected at regular intervals of the time throughout the photocatalytic experiments and degradation observed using UV-visible spectroscopy. The results are shown in Fig. 4a and Fig. 4c respectively. These figures indicate that there is no change in absorption maxima of both the dyes in absence of NiO/Cr_2O_3 nanocomposite under 30 min sunlight irradiation. This confirms that the degradation of dyes does not occur in the absence of NiO/Cr_2O_3 photocatalyst under 30 min sunlight exposure. Figure 4b and Fig. 4d demonstrated a significant decrease in the absorption maxima of both CV and MB organic dyes under sunlight irradiation for 30 min and 180 min respectively (absorption maximum of CV is at 580 nm and absorption maximum of MB is at 660 nm). By the Beer-Lambert law, the decrease in absorption maxima confirms the reduction in the concentration of dyes with an increase in sunlight exposure time (Patel et al. 2021; Shubha et al. 2021). The synthesized NiO/Cr_2O_3 nanocomposite displays magnificent photocatalytic activity towards CV and MB dyes under sunlight irradiation. We have calculated the degradation efficiency of the NiO/Cr_2O_3 photocatalyst for both CV and MB dyes using Eq. (2). Equation (2) is reported in the literature (Pirzada et al. 2019).

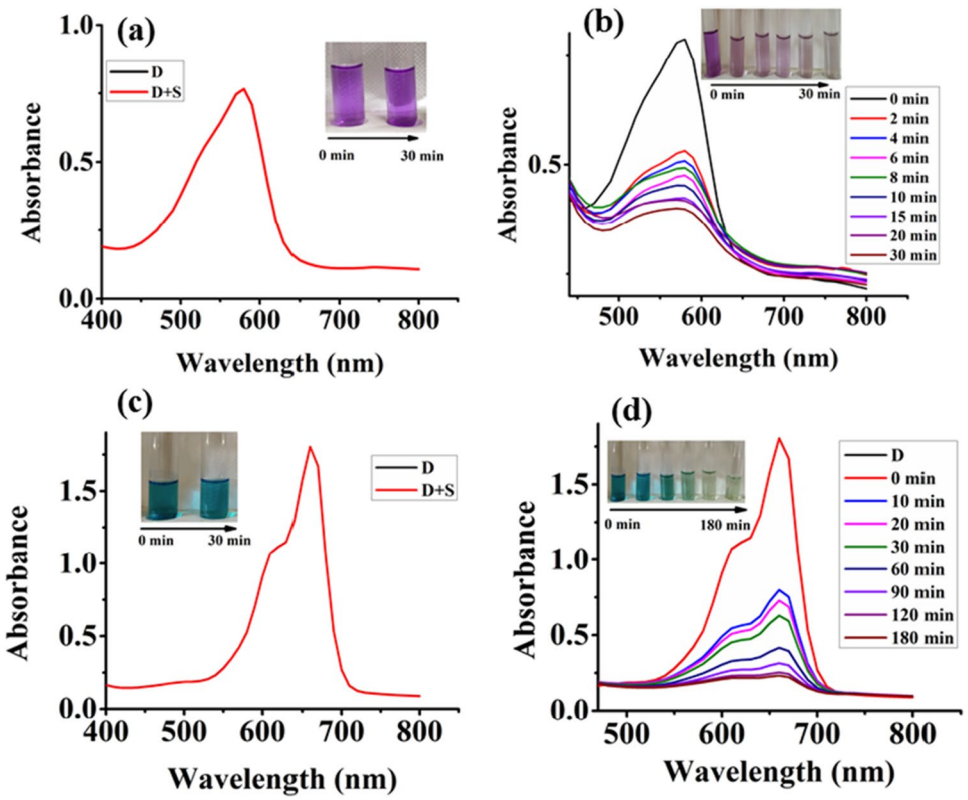

Fig. 4 The UV-visible spectrum of (**a**) CV dye samples in absence of NiO/Cr_2O_3 nanocomposite under 30 min sunlight irradiation, (**b**) CV dye samples in presence of NiO/Cr_2O_3 nanocomposite under 30 min sunlight irradiation, (**c**) MB dye samples in absence of NiO/Cr_2O_3 nanocomposite under 30 min sunlight irradiation, and (**d**) MB dye samples in presence of NiO/Cr_2O_3 nanocomposite under 180 min sunlight irradiation

$$\text{Efficiency}\% = \left(\frac{(C_0 - C_t)}{C_o}\right) \times 100 \quad (2)$$

Here, C_0 is the initial concentration of dyes, and C_t is the concentration of dyes at different intervals of time in the photocatalytic reaction. The calculated efficiency of NiO/Cr_2O_3 photocatalyst for CV has been obtained at 58.10 % within 2 min of sunlight irradiation. 88.47 % degradation of CV has been observed after 30 min of sunlight irradiation in presence of photocatalyst. Photocatalytic degradation efficiencies of the above photocatalyst for MB are 59.90 % within 30 min of sunlight irradiation and 93.63 % within 180 min of sunlight irradiation. The results exhibit that NiO/Cr_2O_3 nanocomposite acts as an efficient photocatalyst for the degradation of both CV and MB dyes under sunlight exposure. Present work is improved in terms of a light source, irradiation time, and degradation efficiency compared to other photocatalysts. For example, SnSe nanocrystal has been reported with 88.68 % degradation of MB dye and 98 % degradation of CV dye under 360 min of UV light irradiation (Patel et al. 2021) and $K_2Ti_6O_{13}$ nanoparticles have been reported with 79.23 % degradation of MB dye under 105 min UV light exposure (Somashekharappa and Lokesh 2021). NiO/Co_3O_4 nanocomposite has also been studied for (89.88%) degradation of methylene blue under sunlight within 360 min (Yadav et al. 2022).

The photocatalytic degradation efficiencies of NiO/Cr_2O_3 photocatalyst against CV and MB dyes are given in Table 2. A comparative study on the photocatalytic activity of earlier

Table 2 The photocatalytic efficiency of synthesized NiO/Cr_2O_3 nanocomposite for CV and MB at different times of sunlight irradiation

Dye	Time (min)	Percentage (%) of dye degradation	Source
Crystal violet	2	58.10	Sunlight
Crystal violet	4	63.47	Sunlight
Crystal violet	6	66.32	Sunlight
Crystal violet	8	70.86	Sunlight
Crystal violet	10	76.16	Sunlight
Crystal violet	15	82.71	Sunlight
Crystal violet	20	84.08	Sunlight
Crystal violet	30	88.47	Sunlight
Methylene blue	10	59.90	Sunlight
Methylene blue	20	64.10	Sunlight
Methylene blue	30	70.01	Sunlight
Methylene blue	60	82.70	Sunlight
Methylene blue	90	88.74	Sunlight
Methylene blue	120	92.39	Sunlight
Methylene blue	180	93.63	Sunlight

reported photocatalyst with NiO/Cr_2O_3 photocatalyst against CV and MB dyes is given in Table 3.

A possible photocatalytic reaction mechanism can be explained with help of the formation of electron-hole pairs on the surface of the NiO/Cr_2O_3 photocatalyst. Sunlight exposure excites electrons from the valance band to the conduction band to get an electron-hole pair on the surface of the photocatalyst. In detail, electrons from the conduction band of nanocomposite NiO/Cr_2O_3 react with an O_2 molecule to produce ($O_2^{\bullet-}$) superoxide radical and holes from the valance band react with an H_2O molecule to produce (OH^-) hydroxyl anion. Hydroxyl anion further reacts with the hole to produce ($OH^{\bullet}$) hydroxyl radical. Finally, this highly reactive hydroxyl radical is responsible for the degradation of CV and MB dye molecules (Patel et al. 2021; Somashekharappa and Lokesh 2021; Sanakousar et al. 2021). A graphical representation of possible general photocatalytic reaction mechanism for the degradation of organic dyes using metal oxide semiconductors based photocatalysts is given in Fig. 5. Morphology has an important influence on the photocatalytic activity of semiconductor photocatalysts. The reason behind this is the dependence of the surface area/surface active site of a photocatalyst. Herein, NiO/Cr_2O_3 photocatalyst has high surface active sites (surface area) because of the presence of cracks on its surface. High surface active sites help in increasing the adsorption of dye molecules on the surface of the photocatalyst. This increased adsorption of dye molecules on the surface of NiO/Cr_2O_3 photocatalyst is responsible for enhanced photocatalytic activity against

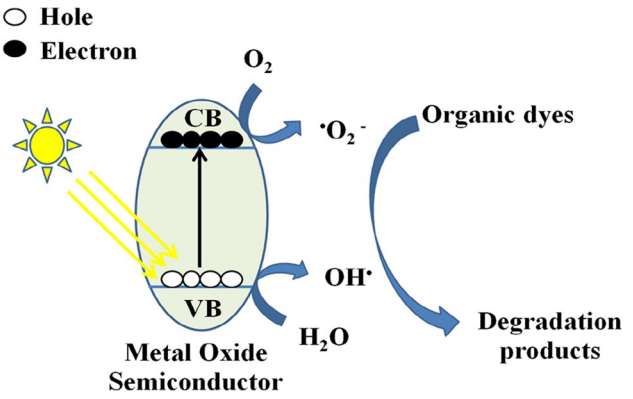

Fig. 5 A graphical representation of possible general photocatalytic reaction mechanism for the degradation of organic dyes using metal oxide semiconductors based photocatalysts (Tayyab et al 2022), Copyright © 2022 Dalian Institute of Chemical Physics, the Chinese Academy of Sciences. Published by Elsevier B.V. All rights reserved, copied with permission

CV and MB dye solution under sunlight exposure. A similar example is reported in the literature. Where, nano-cracks present in the CeO_2-TiO_2 hybrid nanostructure show better photocatalytic activity against MB dye than CeO_2-TiO_2 hybrid nanostructure without nano-cracks (Veziroglu et al. 2019).

A kinetic study of photocatalytic degradation of crystal violet (CV) and methylene blue (MB) dye solutions using NiO/Cr_2O_3 nanocomposite is given in Fig. 6a and Fig. 6b. We have used Eq. (3) for the calculation of photodegradation

Table 3 Comparative study of earlier reported photocatalytic behavior of various photocatalysts with present work against crystal violet (CV) and methylene blue (MB) dyes

S.N.	Photocatalysts	Synthesis techniques	Light source of irradiation/time of irradiation	Dye/degradation efficiency %	References
1	SnSe nanocrystal	Sonochemical exfoliation technique	UV light/360 min	MB/88.68 % and CV/98 %	(Patel et al. 2021)
2	$ZnO/Eu_2O_3/NiO$	One-pot combustion method	Sunlight/150 min	MB/97 %	(Shubha et al. 2021)
3	TiO_2/polyvinyl alcohol/cork nanocomposite	Sol-gel method	Visible light/120 min	MB/98.43 %	(Idris et al. 2021)
4	$K_2Ti_6O_{13}$ nanotubes	Hydrothermal synthesis	UV light/90 min	MB/82.06 %	(Somashekharappa and Lokesh 2021)
5	$K_2Ti_6O_{13}$ nanoparticles	Hydrothermal synthesis	UV light/105 min	MB/79.23 %	(Somashekharappa and Lokesh 2021)
6	0.5 mol% Cd doped ZnO nanoparticles	Precipitation method	UV chamber(0.6 W)/30 min	CV/100 %	(Sanakousar et al. 2021)
7	ZnO/GO nanohybrid	Co-precipitation method	Visible light/240 min	CV/99 %	(Puneetha et al. 2021)
8	NiO nanoparticles	Biosynthesis method	Sunlight/105 min	CV/99 %	(Aminuzzaman et al. 2021)
9	In_2O_3 nanocapsule	Biogenic reflux method	Sunlight/180 min	CV/90 %	(Pawar et al. 2020)
10	NiO/ Cr_2O_3 nanocomposite	Chemical reduction method	Sunlight/30 min	CV/88.47 %	This work
11	NiO/ Cr_2O_3 nanocomposite	Chemical reduction method	Sunlight/180 min	MB/93.63 %	This work

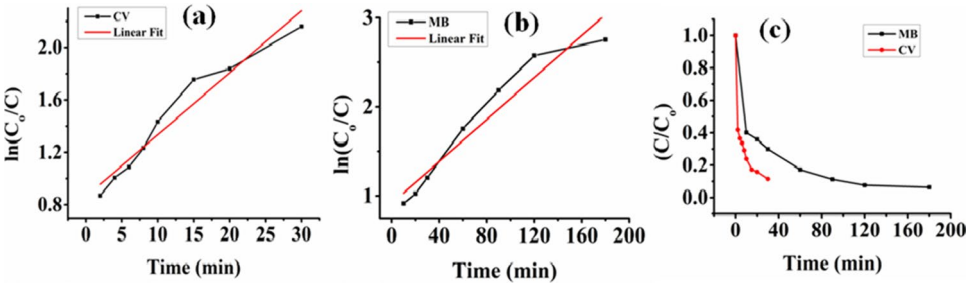

Fig. 6 Kinetics of photocatalytic degradation of (**a**) crystal violet (CV) dye with NiO/Cr_2O_3 nanocomposite, (**b**) methylene blue (MB) dye with NiO/Cr_2O_3 nanocomposite, and (**c**) C/C_0 vs. time of irradiation plot for photocatalytic efficiency NiO/Cr_2O_3 nanocomposite against CV and MB dyes under sunlight exposure

rates of CV and MB dyes in presence of synthesized photocatalyst. Equation (3) is given in the literature (Somashekharappa and Lokesh 2021). The linear fitted straight lines (Fig. 6a and Fig. 6b) confirm the pseudo-first-order reaction kinetics for the above photocatalytic reaction (Idris et al. 2021).

$$\ln\left(\frac{C_o}{C_t}\right) = -kt \tag{3}$$

Where C_0 is the initial concentration of dye solutions, C_t is the concentration of dye solutions at time interval t, k is rate constant (min^{-1}) and t is the time of irradiation of sunlight. The observed rate constant values for NiO/Cr_2O_3 nanocomposite were 0.04732 min^{-1} and 0.01179 min^{-1} against crystal violet and methylene blue organic dyes respectively. Rate constant data suggest that NiO/Cr_2O_3 nanocomposite has a higher rate of degradation for crystal violet than methylene blue organic dyes under sunlight exposure. A plot between C/C_0 vs. time of irradiation is given in Fig. 6c. It is clear from the graph that the degradation efficiency of CV is better than MB dyes in the presence of NiO/Cr_2O_3 nanocomposite. Finally, the results displayed that NiO/Cr_2O_3 nanocomposite has excellent photocatalytic activities for both crystal violet and methylene blue dye solutions under the irradiation of natural sunlight. NiO/Cr_2O_3 nanocomposite shows a better photocatalytic reaction rate for crystal violet dye solution than the methylene blue dye solution.

The reusability of synthesized NiO/Cr_2O_3 nanocomposite was studied and illustrated in Fig. 7a and b. This photocatalyst has shown 79.68 % of CV dye degradation in second cycle and 74.47 % of CV dye degradation in fifth cycle (within 30 min of sunlight irradiation). Synthesized NiO/Cr_2O_3 nanocomposite has shown 93.38 % of MB dye degradation in second cycle and 86.34 % of MB dye degradation in fifth cycle (with in 180 min of sunlight irradiation). Also, Fig. 7c and d illustrated the TEM images of synthesized NiO/Cr_2O_3 nanocomposite after the photocatalytic degradation of CV and MB dyes respectively. The TEM images reveal that the synthesized NiO/Cr_2O_3 nanocomposite is stable after five cycles of photocatalytic reaction. Consequently, it is clear that synthesized NiO/Cr_2O_3 nanocomposite exhibited excellent reusability and stability for photocatalytic degradation of both the organic dyes under sunlight exposure.

Photoelectrochemical measurements of NiO/Cr_2O_3 nanocomposite

Photoelectrochemical measurements of synthesized NiO/Cr_2O_3 nanocomposite are given in Fig. 8. The transient photocurrent spectrum (Fig. 8a) reveals that the current of synthesized NiO/Cr_2O_3 nanocomposite modified stainless steel electrode was increased very fast in solar light irradiation than dark conditions. This increase in photocurrent/photoconductivity is because of rapid formation and movement of electron-hole pair under solar light irradiation. This consequently leads to better photocatalytic activity of synthesized NiO/Cr_2O_3 nanocomposite. Similar results are given in literature (Cui et al. 2018; Tayyab et al. 2022). The EIS Nyquist plot (Fig. 8b) of synthesized NiO/Cr_2O_3 nanocomposite shows very small diameter of the semicircle (the semicircle is observed at high frequency region). The small diameter of the semicircle indicated that small charge transfer resistance. This confirms that synthesized NiO/Cr_2O_3 nanocomposite has increased electron-hole separation for enhanced photocatalytic activity under solar light as reported in literature (Wang et al. 2020). Figure 8c shows Mott-Schottky plot of synthesized NiO/Cr_2O_3 nanocomposite. The negative slope of Mott-Schottky plot confirms that synthesized NiO/Cr_2O_3 nanocomposite is a p-type semiconductor. We have also observed the flat band potential (V_{FB}) of synthesized NiO/Cr_2O_3 nanocomposite by extrapolating the linear portion of Mott-Schottky plot (Wang et al. 2020). The observed V_{FB} value of synthesized NiO/Cr_2O_3 nanocomposite is +1.01 V with reference to Ag/AgCl electrode. The V_{FB} value of p-type semiconductor is generally

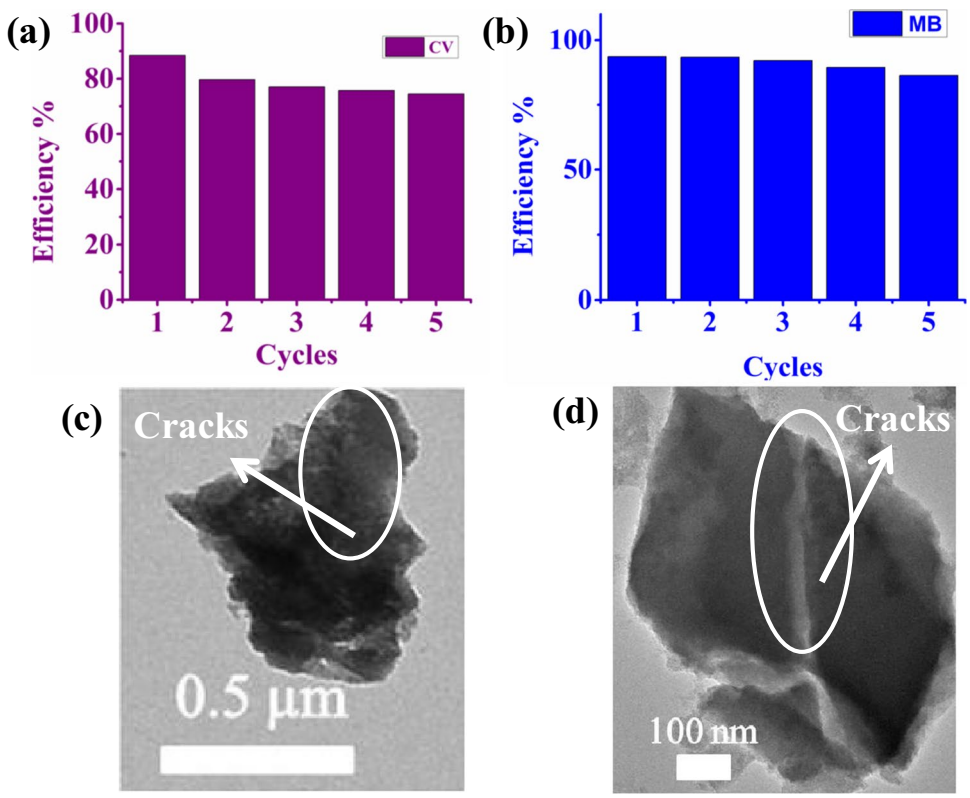

Fig. 7 (**a**), (**b**) Five cycles of photodegradation of CV dye and MB dyes respectively using NiO/Cr_2O_3 nanocomposite, (**c**) and (**d**) TEM images of NiO/Cr_2O_3 nanocomposite after photodegradation of CV dye and MB dye respectively

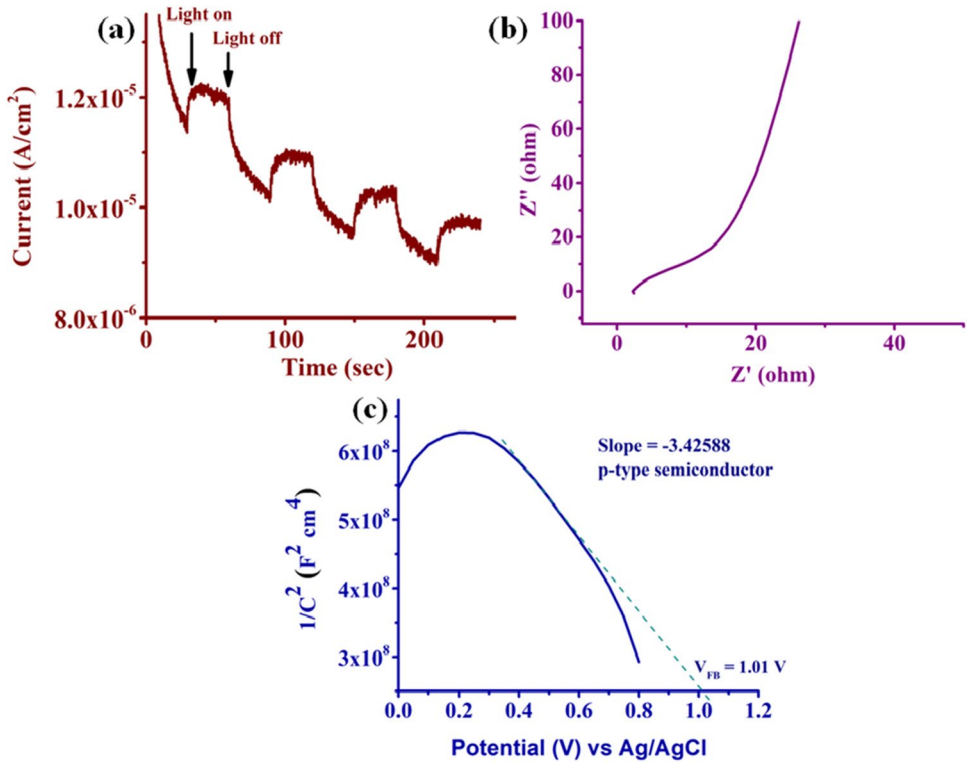

Fig. 8 (**a**) Transient photocurrent, (**b**) the EIS Nyquist plot, and (**c**) electrochemical Mott-Schottky plot of synthesized NiO/Cr_2O_3 nanocomposite

considered as approximate equal to the VB edge potential (Wang et al. 2020). The above photoelectrochemical study supports the enhanced photocatalytic activity of synthesized NiO/Cr_2O_3 nanocomposite against organic dyes degradation under sunlight irradiation.

Conclusion

In summary, NiO/Cr_2O_3 nanocomposite has been successfully fabricated by a simple chemical reduction method. Synthesized nanocomposite has been characterized using PXRD, SEM, TEM, EDS, elemental mapping, FTIR, and UV-visible spectroscopy. The PXRD and EDS analysis confirmed the presence of both NiO and Cr_2O_3 crystal phases in the synthesized photocatalyst. Nano to micro size cracked morphology of synthesized NiO/Cr_2O_3 nanocomposite was observed by SEM analysis. Synthesized photocatalyst exhibits high photocatalytic efficiencies of 88.47 % for crystal violet in 30 min sunlight exposure and 93.63 % for methylene blue in 180 min sunlight exposure. The photocatalytic degradation occurred for both the dyes and following the pseudo-first-order kinetics. The calculated rate constant values are 0.04732 min^{-1} for crystal violet degradation and 0.01179 min^{-1} for methylene blue degradation. We have also performed reusability tests of synthesized photocatalysts up to 5 cycles. NiO/Cr_2O_3 nanocomposite exhibited excellent reusability and stability for photocatalytic degradation of both methylene blue and crystal violet dyes. The synthesized NiO/Cr_2O_3 nanocomposite has been characterized photoelectrochemically using the photocurrent, EIS, and Mott-Schottky plot. The photoelectrochemical analysis supported the enhanced photocatalytic behavior of synthesized NiO/Cr_2O_3 nanocomposite for organic dye degradation under sunlight exposure. Thus, NiO/Cr_2O_3 nanocomposite is proved to be an effective photocatalyst for the degradation of crystal violet and methylene blue under sunlight irradiation.

Abbreviations GO: graphene oxide; MWCNTs: multi-walled carbon nanotubes; SWCNTs: singled-walled carbon nanotubes; SEM: scanning electron microscopy; TEM: transmission electron microscopy; EIS: electrochemical impedance spectroscopy; EDX: energy-dispersive X-ray; ATR-FT-IR: attenuated total reflections Fourier transform infrared spectrometer; PXRD: powder X-ray diffraction technique; CV: crystal violet; MB: methylene blue

Acknowledgements The authors highly acknowledge Principal, Miranda House, University of Delhi for necessary laboratory facilities. The authors thank USIC, University of Delhi for instrumental facilities. The authors acknowledge IUAC, New Delhi for TEM facility. The authors also thank Mr. Himanshu Gupta, Department of Physics, Malaviya National Institute of Technology Jaipur, JLN Marg, Jaipur - 302017, Rajasthan, India, for helping in taking the photoelectrochemical measurements. Sapna Yadav presents her sincere thanks to CSIR, New Delhi (CSIR File No. 08/700(0004)/2019-EMR-I) for a senior research fellowship.

Author contribution Conceptualization; Kalawati Saini, methodology writing-original draft; Sapna Yadav and Nutan Rani, photoelectrochemical measurements, supervision and editing; Kalawati Saini.

Funding Sapna Yadav would like to express her great appreciation CSIR, New Delhi for JRF (CSIR, File No. 08/700(0004)/2019-EMR-1).

Data availability Not applicable.

Declarations

Ethics approval Not applicable.

Consent to participate All the authors consented to participate in the drafting of this research article.

Consent for publication All of the authors consented to publish this research article.

Conflict of interest The authors declare no competing interests.

References

Abd-Elrahim AG, Chun DM (2021) Room-temperature deposition of ZnO-graphene nanocomposite hybrid photocatalysts for improved visible-light-driven degradation of methylene blue. Ceram Int 47:12812–12825. https://doi.org/10.1016/j.ceramint.2021.01.142

Abukhadra MR, Shaban M, Samad MAAE (2018) Enhanced photocatalytic removal of Safranin-T dye under sunlight within minute time intervals using heulandite/polyaniline@ nickel oxide composite as a novel photocatalyst. Ecotoxicol Environ Saf 162:261–271. https://doi.org/10.1016/j.ecoenv.2018.06.081

Alagiri M, Ponnusamy S, Muthamizhchelvan C (2012) Synthesis and characterization of NiO nanoparticles by sol–gel method. J Mater Sci Mater Electron 23:728–732. https://doi.org/10.1007/s10854-011-0479-6

Al-Hada NM, Al-Ghaili AM, Kasim H, Saleh MA, Baqiah H, Liu J, Wang J (2021) Nanofabrication of $(Cr_2O_3)_x$ $(NiO)_{1-x}$ and the impact of precursor concentrations on nanoparticles conduct. J Mater Res Technol 11:252–263. https://doi.org/10.1016/j.jmrt.2021.01.007

Al-Hada NM, Kamari HM, Saleh MA, Flaifel MH, Al-Ghaili AM, Kasim H, Baqer AA, Saion E, Jihua W (2020) Morphological, structural and optical behaviour of PVA capped binary $(NiO)_{0.5}$ $(Cr_2O_3)_{0.5}$ nanoparticles produced via single step based thermal technique. Results Phys 17:103059. https://doi.org/10.1016/j.rinp.2020.103059

Aminuzzaman M, Chong CY, Goh WS, Phang YK, Lai-Hock T, Chee SY, Akhtaruzzaman M, Ogawa S, Watanabe A (2021) Biosynthesis of NiO nanoparticles using Soursop (*Annona muricata L.*) fruit peel green waste and their photocatalytic performance on crystal violet dye. J Clust Sci 32:949–958. https://doi.org/10.1007/s10876-020-01859-8

Barir R, Benhaoua B, Benhamida S, Rahal A, Sahraoui T, Gheriani R (2017) Effect of precursor concentration on structural optical and electrical properties of NiO thin films prepared by spray pyrolysis. J Nanomater 2017:5204639. https://doi.org/10.1155/2017/5204639

Cui H, Li B, Li Z, Li X, Xu S (2018) Z-scheme based CdS/$CdWO_4$ heterojunction visible light photocatalyst for dye degradation and hydrogen evolution. Appl Surf Sci 455:831–840. https://doi.org/10.1016/j.apsusc.2018.06.054

Dewangan R, Hashmi A, Asthana A, Singh AKM, Susan MABH (2020) Degradation of methylene blue and methyl violet using graphene oxide/NiO/β-cyclodextrin nanocomposites as photocatalyst. Int J Environ Anal Chem 1-20. https://doi.org/10.1080/03067319.2020.1802443

Din MI, Nabi AG, Rani A, Aihetasham A, Mukhtar M (2018) Single step green synthesis of stable nickel and nickel oxide nanoparticles from *Calotropis gigantea*: Catalytic and antimicrobial potentials. Environ Nanotechnol Monit Manag 9:29–36. https://doi.org/10.1016/j.enmm.2017.11.005

Fu Y, Gu H, Yan X, Liu J, Wang Y, Huang J, Li X, Lv H, Wang X, Guo J, Lu G, Qiu S, Guo Z (2015) Chromium(III) oxide carbon nanocomposites lithium-ion battery anodes with enhanced energy conversion performance. Chem Eng J 277:186–193. https://doi.org/10.1016/j.cej.2015.04.142

Guillén C, Herrero J (2021) Structural changes induced by heating in sputtered NiO and Cr_2O_3 thin films as p-type transparent conductive electrodes. Electron Mater 2:49–59. https://doi.org/10.3390/electronicmat2020005

Hassanpour M, Safardoust-Hojaghan H, Salavati-Niasari M (2017) Degradation of methylene blue and Rhodamine B as water pollutants via green synthesized Co_3O_4/ZnO nanocomposite. J Mol Liq 229:293–299. https://doi.org/10.1016/j.molliq.2016.12.090

He H, Yang S, Yu K, Ju Y, Sun C, Wang L (2010) Microwave induced catalytic degradation of crystal violet in nano-nickel dioxide suspensions. J Hazard Mater 173:393–400. https://doi.org/10.1016/j.jhazmat.2009.08.084

Hema M, Arasi AY, Tamilselvi P, Anbarasan R (2013) Titania nanoparticles synthesized by sol-gel technique. Chem Sci Trans 2(1):239–245. https://doi.org/10.7598/cst2013.344

Hong WG, Kim BH, Lee SM, Yu HY, Yun YJ, Jun Y, Lee JB, Kim HJ (2012) Agent-free synthesis of graphene oxide/transition metal oxide composites and its application for hydrogen storage. Int J Hydrog Energy 37:7594–7599. https://doi.org/10.1016/j.ijhydene.2012.02.010

Hou J, Wang Y, Zhou J, Lu Y, Liu Y, Lv X (2021) Photocatalytic degradation of methylene blue using a ZnO/TiO_2 heterojunction nanomesh electrode. Surf Interfaces 22:100889. https://doi.org/10.1016/j.surfin.2020.100889

Idris NHM, Rajakumar J, Cheong KY, Kennedy BJ, Ohno T, Yamakata A, Lee HL (2021) Titanium dioxide/polyvinyl alcohol/cork nanocomposite: a floating photocatalyst for the degradation of methylene blue under irradiation of a visible light source. ACS Omega 6:14493–14503. https://doi.org/10.1021/acsomega.1c01458

Krishna YVSS, Sandhya G, Babu RR (2018) Removal of heavy metals Pb(II), Cd(II) and Cu(II) from waste waters using synthesized chromium doped nickel oxide nanoparticles. Bull Chem Soc Ethiop 32(2):225–238. https://doi.org/10.4314/bcse.v32i2.4

Li F, Huang X, Jiang Y, Liu L, Li Z (2009) Synthesis and characterization of ZnO/SiO_2 core/shell nanocomposites and hollow SiO_2 nanostructures. Mater Res Bull 44:437–441. https://doi.org/10.1016/j.materresbull.2008.04.024

Liang Q, Ma W, Shi Y, Li Z, Yang X (2012) Hierarchical Ag_3PO_4 porous microcubes with enhanced photocatalytic properties synthesized with the assistance of trisodium citrate. Cryst Eng Comm 14:2966. https://doi.org/10.1039/c2ce06425a

Liu G, Feng M, Tayyab M, Gong J, Zhang M, Yang M, Lin K (2021a) Direct and efficient reduction of perfluorooctanoic acid using bimetallic catalyst supported on carbon. J Hazard Mater 412:125224. https://doi.org/10.1016/j.jhazmat.2021.125224

Liu Y, Zhu Q, Tayyab M, Zhou L, Lei J, Zhang J (2021b) Single-atom Pt loaded zinc vacancies ZnO–ZnS induced type-V electron transport for efficiency photocatalytic H_2 evolution. RRL Solar 5(11):2100536. https://doi.org/10.1002/solr.202100536

Liu X, Wang J, Yang G (2018) Amorphous nickel oxide and crystalline manganese oxide nanocomposite electrode for transparent and flexible supercapacitor. Chem Eng J 347:101–110. https://doi.org/10.1016/j.cej.2018.04.070

Ma J, Ding J, Yu L, Li L, Kong Y, Komarneni S (2015) Synthesis of Fe_2O_3–NiO–Cr_2O_3 composites from NiFe-layered double hydroxide for degrading methylene blue under visible light. Appl Clay Sci 107:85–89. https://doi.org/10.1016/j.clay.2015.01.007

Madkour M, Abdel-Monem YK, Sagheer FA (2016) Controlled synthesis of NiO and Co_3O_4 nanoparticles from different coordinated precursors: impact of precursor's geometry on the nanoparticles characteristics. Ind Eng Chem Res 55:12733–12741. https://doi.org/10.1021/acs.iecr.6b03231

Mahendiran M, Mathen JJ, Racik M, Madhavan J, Raj MVA (2019) Investigation of structural, optical and electrical properties of transition metal oxide semiconductor CdO-ZnO nanocomposite and its effective role in the removal of water contaminants. J Phys Chem Solids 126:322–334. https://doi.org/10.1016/j.jpcs.2018.11.012

Maheshwaran G, Selvi C, Kaliammal R, Prabhu MR, Kumar MK, Sudhahar S (2021) Exploration of Cr_2O_3-NiO nanocomposite as a superior electrode material for supercapacitor applications. Mater Lett 300:130191. https://doi.org/10.1016/j.matlet.2021.130191

Mohammad EJ, Kareem MM, Lafta AJA (2020) Preparation of MWCNTS/Cr_2O_3-NiO nanocomposite for adsorption and photocatalytic removal of bismarck brown G dye from aqueous solution. Indones J Chem 20(3):554–566. https://doi.org/10.22146/ijc.43429

Patel K, Parangi T, Solanki GK, Mishra MK, Patel KD, Pathak VM (2021) Photocatalytic degradation of methylene blue and crystal violet dyes under UV light irradiation by sonochemically synthesized CuSnSe nanocrystals. Eur Phys J Plus 136:743. https://doi.org/10.1140/epjp/s13360-021-01725-0

Pawar KK, Chaudhary LS, Mali SS, Bhat TS, Sheikh AD, Hong CK, Patil PS (2020) In_2O_3 nanocapsules for rapid photodegradation of crystal violet dye under sunlight. J Colloid Interface Sci 561:287–297. https://doi.org/10.1016/j.jcis.2019.10.101

Pirzada BM, Pushpendra KRK, Naidu BS (2019) Synthesis of $LaFeO_3$/Ag_2CO_3 nanocomposites for photocatalytic degradation of rhodamine B and p-chlorophenol under natural sunlight. ACS Omega 4:2618–2629. https://doi.org/10.1021/acsomega.8b02829

Puneetha J, Kottam N, Ab R (2021) Investigation of photocatalytic degradation of crystal violet and its correlation with bandgap in ZnO and ZnO/GO nanohybrid. Inorg Chem Commun 125:108460. https://doi.org/10.1016/j.inoche.2021.108460

Rahimi-Nasarabadi M, Ahmadi F, Hamdi S, Eslami N, Didehban K, Ganjali MR (2016) Preparation of nanosized chromium carbonate and chromium oxide green pigment through direct carbonation and precursor thermal decomposition. J Mol Liq 216:814–820. https://doi.org/10.1016/j.molliq.2016.01.065

Rahman MM, Balkhoyor HB, Asiri AM, Sobahi TR (2016) Development of selective chloroform sensor with transition metal oxide nanoparticle/multi-walled carbon nanotube nanocomposites by modified glassy carbon electrode. J Taiwan Inst Chem Eng 66:336–346. https://doi.org/10.1016/j.jtice.2016.06.004

Rani M, Yadav J, Shanker U (2021) Green synthesis, kinetics and photoactivity of novel nickel oxide-decorated zinc hexacyanocobaltate catalyst for efficient removal of toxic Cr(VI). J Environ Chem Eng 9:105073. https://doi.org/10.1016/j.jece.2021.105073

Ranjith R, Renganathan V, Chen SM, Selvan NS, Rajam PS (2019) Green synthesis of reduced graphene oxide supported TiO_2/Co_3O_4 nanocomposite for photocatalytic degradation of methylene blue and crystal violet. Ceram Int 45:12926–12933. https://doi.org/10.1016/j.ceramint.2019.03.219

Sanakousar MF, Vidyasagar CC, Jiménez-Pérez VM, Jayanna BK, Mounesh SAH, Prakash K (2021) Efficient photocatalytic degradation of crystal violet dye and electrochemical performance of modified MWCNTs/Cd-ZnO nanoparticles with quantum chemical calculations. J Hazard Mater Adv 2:100004. https://doi.org/10.1016/j.hazadv.2021.100004

Shubha JP, Adil SF, Khan M, Hatshan MR, Khan A (2021) Facile fabrication of a ZnO/Eu_2O_3/NiO-based ternary heterostructure nanophotocatalyst and its application for the degradation of methylene blue. ACS Omega 6:3866–3874. https://doi.org/10.1021/acsomega.0c05670

Singh KK, Senapati KK, Borgohain C, Sarma KC (2017) Newly developed Fe_3O_4–Cr_2O_3 magnetic nanocomposite for photocatalytic decomposition of 4-chlorophenol in water. J Environ Sci 52:333–340. https://doi.org/10.1016/j.jes.2015.01.035

Somashekharappa KK, Lokesh SV (2021) Hydrothermal synthesis of $K_2Ti_6O_{13}$ nanotubes/nanoparticles: a photodegradation study on methylene blue and rhodamine B dyes. ACS Omega 6:7248–7256. https://doi.org/10.1021/acsomega.0c02087

Srirattanapibul S, Nakarungsee P, Issro C, Tang IM, Thongmee S (2022) Performance of NiO intercalated rGO nanocomposites for NH_3 sensing at room temperature. Mater Sci Semicond Process 137:106221. https://doi.org/10.1016/j.mssp.2021.106221

Tayyab M, Liu Y, Min S, Irfan RM, Zhu Q, Zhou L, Lei J, Zhang J (2022) Simultaneous hydrogen production with the selective oxidation of benzyl alcohol to benzaldehyde by a noble-metal-free photocatalyst VC/CdS nanowires. Chin J Catal 43:1165–1175. https://doi.org/10.1016/S1872-2067(21)63997-9

Veziroglu S, Röder K, Gronenberg O, Vahl A, Polonskyi O, Strunskus T, Rubahn HG, Kienle L, Adam J, Fiutowski J, Faupel F, Aktas OC (2019) Cauliflower-like CeO_2–TiO_2 hybrid nanostructures with extreme photocatalytic and self-cleaning properties. Nanoscale 11:9840. https://doi.org/10.1039/c9nr01208g

Wang Y, Yang H, Sun X, Zhang H, Xian T (2020) Preparation and photocatalytic application of ternary n-$BaTiO_3$/Ag/p-AgBr heterostructured photocatalysts for dye degradation. Mater Res Bull 124:110754. https://doi.org/10.1016/j.materresbull.2019.110754

Yadav S, Yadav J, Kumar M, Saini K (2022) Synthesis and characterization of nickel oxide/cobalt oxide nanocomposite for effective degradation of methylene blue and their comparative electrochemical study as electrode material for supercapacitor application. Int. J. Hydrog. Energy In Press. https://doi.org/10.1016/j.ijhydene.2022.02.011

Zhang L, Ran J, Qiao SZ, Jaronie M (2019) Characterization of semiconductor photocatalysts. Chem Soc Rev 48:5184–5206. https://doi.org/10.1039/c9cs00172g

Zhu D, Zhou Q (2019) Action and mechanism of semiconductor photocatalysis on degradation of organic pollutants in water treatment: a review. Environ Nanotechnol Monit Manag 12:100255. https://doi.org/10.1016/j.enmm.2019.100255

Zoromba MS, Bassyouni M, Abdel-Aziz MH, Al-Hossainy AF, Salah N, Al-Ghamdi AA, Eid MR (2019) Structure and photoluminescence characteristics of mixed nickel–chromium oxides nanostructures. Appl Phys A Mater Sci Process 125:642. https://doi.org/10.1007/s00339-019-2933-x